Contents lists available at ScienceDirect

Electrochemistry Communications

Short communication

Template-based electrodeposition and characterization of niobium nanowires

Kirsten Blagg[a,*], Tamara Greymountain[b], Wolfgang Kern[a], Meenakshi Singh[a]

[a] *Colorado School of Mines, Golden, CO 80401, USA*
[b] *Southwestern Indian Polytechnic Institute, Albuquerque, NM, USA*

ABSTRACT

Template-based electrodeposition is a versatile technique for the fabrication of freestanding nanowires. However, nanowires of refractory metals, like niobium, have remained inaccessible via this technique due to preferential hydrogen evolution in aqueous solutions. In this work, we have developed a synthetic strategy for template-based electrodeposition of niobium nanowires using an ionic liquid. Optimal growth conditions have been determined using cyclic voltammetry. Structural characterization using transmission electron microscopy, electron diffraction, and energy dispersive spectroscopy showed that the niobium nanowires were polycrystalline with an average grain size of 14 nm. The use of ionic liquid-based electrolytes for nanowire deposition could be expanded to other metals improving material quality due to their high stability, good conductivity, and wide electrochemical window.

1. Introduction

Nanowires have been the subject of much research in the last three decades due to their unique physical properties and potential applications. Niobium nanowires (NbNWs) in particular have been used to study quantum phase slips [1,2], to form tunnel junctions [3,4,5], and in optical detectors [6,7,8]. For these applications, NbNWs were fabricated using techniques such as sputtering [1,3,7,9], evaporation [5,10,11], and molecular beam epitaxy (MBE) [12] for deposition followed by lithography and etching for patterning. Exotic techniques such as laser ablation in superfluid helium quantum vortices have also been used [13]. These methods are either difficult to control, do not allow for control over sample morphology, are expensive and require specialized equipment, or are limited in scope as the resulting nanowires cannot be manipulated or moved from the fabrication site. Template-based electrodeposition, on the other hand, is a simple, inexpensive fabrication technique that allows for the growth of freestanding nanowires which can be individually manipulated. In addition, sample morphology, diameter, and axial modulation can be controlled using easily tunable growth parameters [14,15,16,17,18]. Here, we have developed a synthetic strategy to grow NbNWs using template-based electrodeposition.

Template-based electrodeposition via aqueous solutions is well understood and has been extensively used to make a variety of nanowires [19]. However, depositing refractory metals such as niobium via aqueous solutions is untenable due to substantial oxygen reduction and hydrogen evolution at the required deposition voltages. Deposition via molten salts has been explored in the past for materials inaccessible via aqueous solutions. While niobium films have been successfully grown using molten salts [20,21,22], the high temperatures required to dissolve molten salts, between 450 °C and 1025 °C, increase corrosion and preclude template-based nanowire fabrication. Recently, ionic liquids have been proposed as an alternative to aqueous solutions and molten salts due to several advantageous properties including low working temperatures, good electrical conductivity, high thermal stability, and wide electrochemical windows [21,23,24]. The electrodeposition of nanowires using ionic liquids has not been explored even though refractory metal films have been successfully deposited using this technique [25,26]. Here, the use of the ionic liquid 1-butyl-1-methylpyrroidinium bis[(trifluoromethyl)sulfonyl]imide ([BMP]TFSA) allows for the deposition of niobium nanowires using template-based electrodeposition. This technique can be expanded to nanowires of other refractory metals which have been inaccessible with traditional methods. Additionally, the quality of materials typically deposited via aqueous solutions can be improved through the use of ionic liquids due to beneficial properties such as a wide electrochemical window.

2. Methods

To avoid moisture contamination, all solution preparation and deposition was done in a nitrogen glove box with both moisture and
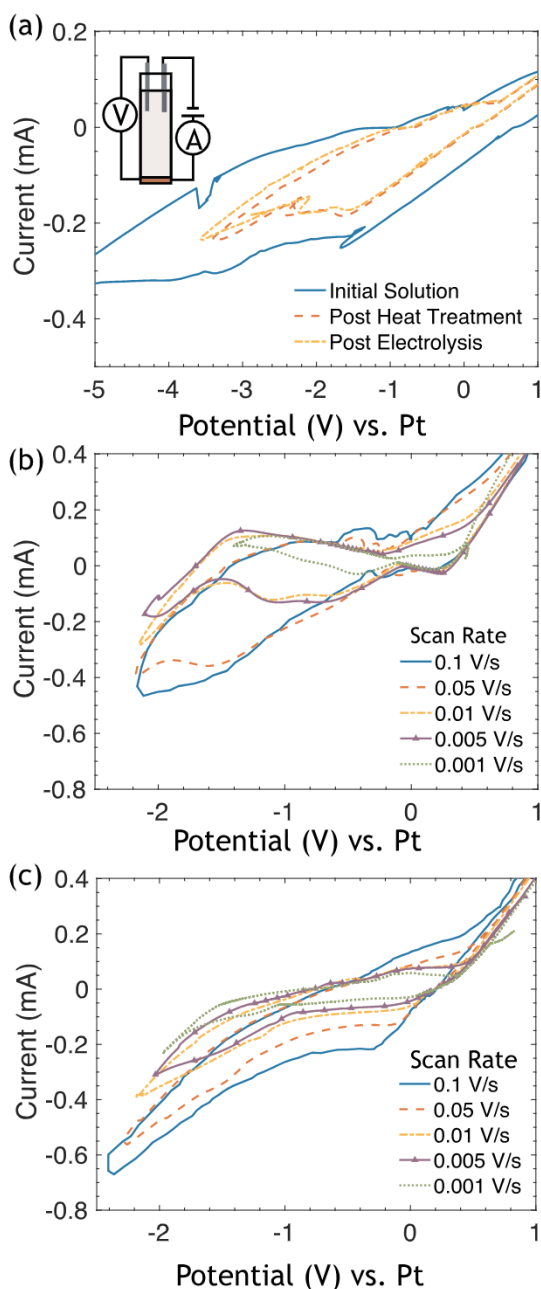
* Corresponding author.
  E-mail address: kblagg@mines.edu (K. Blagg).

Fig. 1. (a) Cyclic voltammetry scan at a rate of 0.10 V/s of ionic liquid [BMP]TFSA at each stage of purification: heating and electrolysis. (inset) Schematic diagram of the electrolytic cell with platinum wires acting as the reference and counter electrodes and a copper plate acting as the working electrode. V and A refer to the measurement of the relevant voltage and current. (b) Cyclic voltammetry scans of the final electrolytic solution containing [BMP]TFSA, NbF$_5$, and NaF is shown for different scan rates. (c) Cyclic voltammetry scans of the final electrolytic solution containing [BMP]TFSA, NbF$_5$, and LiF is shown for different scan rates. BMP[TFSA] residual resistance was subtracted from the cyclic voltammetry plots of the final solutions.

oxygen level below 1 ppm. Additionally, the ionic solution was dried at 125 °C for 24 h on a hotplate and reduced via electrolysis. The reduction of additional contaminants via electrolysis was used to prevent hydrogen evolution during niobium deposition. For electrolysis, a standard three electrode cell with platinum wires acting as the reference and counter electrodes and a thin copper sheet acting as a working electrode was used to set 2 V across the [BMP]TFSA for 7000 s (Fig. 1a inset). The same three electrode set up was then used to characterize the purification process via cyclic voltammetry (CV) with a scan rate of

0.10 V/s (Fig. 1a). The average resistance of the original solution in the region of interest (1 V to 3 V) was 7.74 kΩ and increased to 14.1 kΩ after drying. This 6.36 kΩ increase in resistance is attributed to a decrease in contaminants which act as charge carriers.

The electrolytic solution was prepared by adding 0.25 M NaF or LiF and 0.25 M NbF$_5$ to the purified [BMP]TFSA. The LiF or NaF act as a buffer improving the quality and adherence of the electrodeposit [27,28]. After the addition of each salt, the electrolytic bath was maintained in the glove box at 125 °C for 24 h ensuring that the salt was fully dissolved. CV measurements were performed on the final electrolytic solution using the three electrode setup described above (Fig. 1a inset). The background resistance from the BMP[TFSA] (Fig. 1) was subtracted from the CV plot of the final solution (Fig. 1b and c). For the solution with NaF, two reduction peaks at −0.90 V and −1.94 V are indicative of Nb electroreduction (Fig. 1b) [25,26]. The low voltage current fluctuations present in the CV scans with fast scan rates are likely caused by reaction kinetics. When LiF is used in place of NaF, the reduction peaks shift to −0.27 V and −1.47 V (Fig. 1c). Both CV scans indicate Nb reduction is an irreversible redox reaction. While the relationship between the scan rate and the peak current is described by the Randles-Sevcik equation, the reduction potential shifts with scan rate and the ratio of anodic to cathodic peak current is not equal to one [29].

To fabricate the NbNWs two different membranes were used as templates: 0.2 μm diameter polycarbonate membranes (PCMs, SPI) and 0.2 μm diameter anodized aluminum membranes (AAMs, GE). The membranes were coated on one side with 500 nm of thermally evaporated copper. The membrane with the copper backing replaced the copper plate in the three cell configuration as the working electrode (Fig. 1a inset). At −2.6 V, an increase in current in the CV scan for the NaF solution can be attributed to the complete reduction of niobium (Fig. 1b). As a result, −2.6 V were applied between the working and counter electrode for the final deposition of Nb using the solution of NbF$_5$ and NaF. −1.9 V were applied for the deposition of Nb from the solution of NbF$_5$ and LiF. The Nb was deposited into the template pores at a current density of 0.063 –0.096 A/m^2 at an average rate of 1.6 μm/h.

3. Results and discussion

In order to view and measure individual nanowires, the nanowires were extracted from the membrane using the following procedure. The copper metal was removed from the back of the PCM or AAM using a cotton swab and isopropyl alcohol (IPA). The membrane was then dissolved in either dichloromethane for PCM or 0.1 M NaOH for AAM leaving the NbNWs suspended in solution. The NbNWs were cleaned by repeated cycles of centrifugal separation, replacement of dichloromethane or NaOH with IPA, and sonication in IPA.

The clean NbNWs were dispersed on a lacey carbon mesh grid (SPI) for characterization with transmission electron microscopy (TEM, FEI Talos F200X) and selective area electron diffraction (SAED). The nanowires grown in the PCM have uniform diameter of 200 nm and an average length of 5 μm (Fig. 2a). Those grown in the AAMs have a diameter between 130–170 nm and an average length of 7 μm (Fig. 2b). These wires which were imaged two weeks after removal from the membrane have an oxide layer on average 8.6 nm thick varying 13 nm across an individual wire. Wires imaged two months after removal from the membrane have an oxide layer 53 nm thick which varied 70 nm between samples and 16 nm across an individual wire. In some instances, the oxide had pinched off the niobium.

Energy dispersive spectroscopy (EDS) was used to measure the composition of the nanowire grown using the NaF solution (Fig. 3a upper) and the LiF solution (Fig. 3a lower). For the nanowires deposited using the NaF solution, niobium represents 45% of the total sample in the beam spot. In the case of the LiF solution, niobium represents 55%. Both nanowires show the presence of copper which can be attributed to
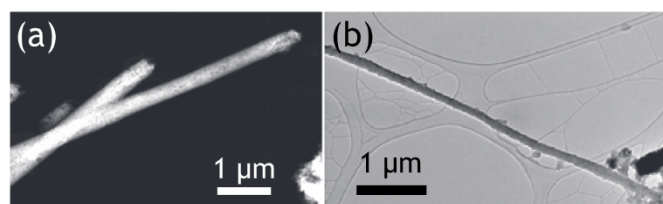
Fig. 2. (a) TEM image of 6 μm long, 200 nm diameter niobium nanowires deposited in a PCM using a solution of [BMP]TFSA, NbF₅, and NaF. (b) TEM image of a 4 μm long, 130 nm diameter niobium nanowire deposited in an AAM using a solution of [BMP]TFSA, NbF₅, and LiF.
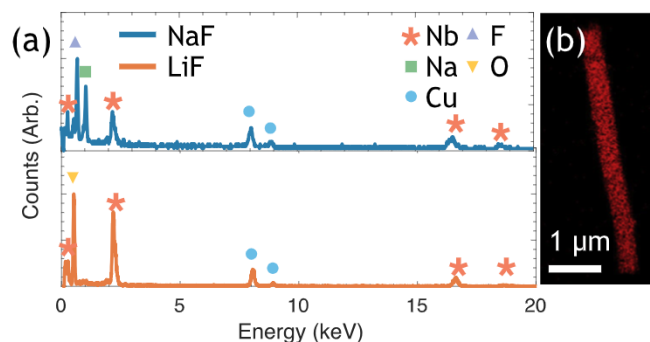

Fig. 3. (a) The blue line represents the EDS spectrum of a nanowire deposited using NaF. In addition to niobium peaks (red star), multiple contaminants are shown. Sodium (green square) and fluorine (purple triangle) peaks indicate contaminants from the niobium deposition. The red line shows the spectra from a nanowire deposited using the LiF solution. In addition to niobium peaks (red star), an oxygen peak (yellow upside down triangle) is also present. The mesh grid leads to the presence of copper peaks (blue circle). (b) EDS mapping of niobium concentration of a single nanowire deposited via NaF is given in red. (For interpretation of the references to color in this figure legend, the reader is referred to the web version of this article.)

Fig. 4. (a) Polycrystalline electron diffraction pattern of niobium nanowire deposited via NaF. (b) Selective dark field image of a niobium nanowire highlighting the crystalline grains.

Fig. 5. (a) Four electrical pads used to connect the nanowire to measurement electronics. (b) Electron microscopy image of niobium nanowire set up in a four probe resistance measurement using FIB deposited platinum. (c) Resistance versus time since removal from the membrane.

the TEM grid. For the nanowires deposited using the NaF solution, fluorine and sodium peaks are also present, accounting for 13% and 28% of the total sample in the beam spot. The nanowires deposited using the LiF solution show 0% F contamination. Any Li contamination cannot be measured via EDS. The fluorine and sodium present in the NaF deposited wires is due to the accumulation of fluorine and sodium ions which were liberated during the reduction steps. In particular, if a slight overpotential is applied, the fluorine and sodium ions are unable to diffuse and accumulate on the deposition surface [28]. The lower deposition voltage used in the case of the LiF solution substantially reduces the fluorine contamination. In the case of the LiF wire, oxygen accounts for 20% of the beam spot corresponding to the formation of an oxide layer. The wires deposited with NaF as a buffer show no oxygen presence as the wires were imaged immediately after removal from the template.

An analysis of the electron diffraction pattern shows the nanowires are polycrystalline with a combination of base-centered cubic and face-centered cubic crystal structures (Fig. 4a). The amorphous niobium oxide does not contribute to the diffraction pattern. An atomic spacing of 2.94 Å [30], compared to the bulk spacing of 3.03 Å, was found. Oxidation and contamination of niobium increases the strain in the crystal lattice and can cause the observed decrease in the lattice spacing [31,32,33]. Dark field imaging indicates an average grain size of 14 nm with the largest grains measuring about 80 nm (Fig. 4b).

To perform four probe resistivity measurements on a single niobium nanowire, four aluminum contacts were fabricated on a silicon/silicon dioxide wafer using photolithography (Shipley 1813, Karl Suss MJB3 mask aligner) and magnetron sputtering of aluminum (Fig. 5a). A drop of the niobium nanowire suspension was dispersed onto the silicon chip. The electrodes were connected to a single niobium nanowire using
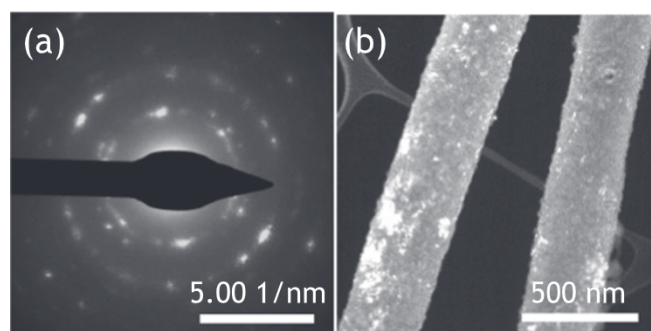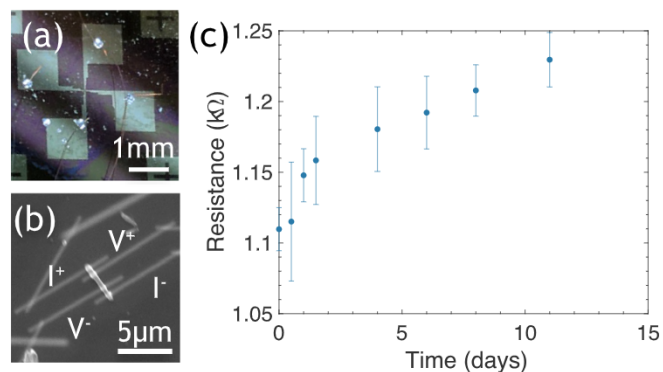
focused ion beam (FIB, FEI Helios Nanolab 600i) platinum deposition (Fig. 5b). The contacts were connected to measurement electronics using silver paint or indium dots (The Indium Corporation) and copper wire.

Room temperature resistance was measured as a function of time since the nanowire was removed from the membrane (Fig. 5c). The resistivity of the nanowire immediately removed from the membrane is 15.2 μΩm compared to the bulk resistivity of 0.115 μΩm for pure niobium. The resistance increases logarithmically ($y = 0.33 \log(x) + 1.14$) from 1.1 kΩ to 1.23 kΩ in 11 days (Fig. 5c). This 11 Ω/day increase corresponds to an average oxidation growth of 0.73 nm/day. This is significantly faster than the 0.1 nm/3 days oxidation of bulk ultra pure niobium [33]. The oxidation of niobium occurs through a process of nucleation and segregation [32,33,34,35]. The strain due to defects and grain boundaries provides a segregation site leading to enhanced oxygen concentration and rapid oxidation [31,33,36,37]. The rapid oxidation rate of niobium nanowires is attributed to the polycrystallinity, defects, and increased surface to volume ratio.

4. Conclusion

We have shown for the first time the growth of niobium nanowires via template-based electrodeposition. The use of the ionic liquid [BMP]TFSA with NbF₅ and NaF or LiF avoids the technical challenges that make deposition from aqueous solutions or molten salts impossible. TEM, SAED, and EDS show the NbNWs were polycrystalline, 130 nm to 200 nm in diameter, and on average 6 μm long. The replacement of NaF with LiF as a buffer solution decreases the deposition voltage and reduces nanowire contamination. Resistivity measurements show the nanowires are sensitive to oxidation. The use of template-based

electrodeposition allows for the simple inexpensive fabrication of freestanding nanowires. Additionally, this technique can be expanded to other refractory metals which have remained inaccessible via traditional methods.

Acknowledgments

References

[1] W. Zhao, X. Liu, M.H.W. Chan, Quantum phase slips in 6 mm long niobium nanowire, Nano Lett. 16 (2) (2016) 1173–1178, https://doi.org/10.1021/acs.nanolett.5b04473.

[2] M. Trezza, C. Cirillo, P. Sabatino, G. Carapella, S.L. Prischepa, C. Attanasio, M. Trezza, C. Cirillo, P. Sabatino, G. Carapella, S.L. Prischepa, C. Attanasio, Nonlinear current-voltage characteristics due to quantum tunneling of phase slips in superconducting Nb nanowire networks, Appl. Phys. Lett. 103 (25) (2013) 252601, https://doi.org/10.1063/1.4851240.

[3] M.D. Henry, S. Wolfley, T. Monson, R. Lewis, Ga lithography in sputtered niobium for superconductive micro and nanowires, Appl. Phys. Lett. 105 (7) (2014) 072601, https://doi.org/10.1063/1.4893446.

[4] D. Olaya, P.D. Dresselhaus, S.P. Benz, S. Member, J. Bjarnason, E.N. Grossman, Amorphous Nb-Si barrier junctions for voltage standard and digital applications, IEEE Trans. Appl. Supercond. 19 (3) (2009) 144–148, https://doi.org/10.1109/TASC.2009.2018254.

[5] Y. Harada, D.B. Haviland, P. Delsing, C.D. Chen, T. Claeson, Fabrication and measurement of a Nb based superconducting single electron transistor, Appl. Phys. Lett. 65 (5) (1994) 636–638, https://doi.org/10.1063/1.112255.

[6] C.M. Natarajan, M.G. Tanner, R.H. Hadfield, Superconducting nanowire single-photon detectors: physics and applications, Supercond. Sci. Technol. 25 (6) (2012) 063001, https://doi.org/10.1088/0953-2048/25/6/063001.

[7] A.J. Annunziata, D.F. Santavicca, J.D. Chudow, L. Frunzio, M.J. Rooks, A. Frydman, D.E. Prober, Niobium superconducting nanowire single-photon detectors, IEEE Trans. Appl. Supercond. 19 (3) (2009) 327–331, https://doi.org/10.1109/TASC.2009.2018740.

[8] K. Inderbitzin, A. Engel, A. Schilling, K. Il, M. Siegel, An ultra-fast superconducting Nb nanowire single-photon detector for soft X-rays, Appl. Phys. Lett. 101 (16) (2012) 162601, https://doi.org/10.1063/1.4759046.

[9] A. Rogachev, A. Bezryadin, Superconducting properties of polycrystalline Nb nanowires templated by carbon nanotubes, Appl. Phys. Lett. 83 (3) (2003) 512–514, https://doi.org/10.1063/1.1592313.

[10] N. Kim, K. Hansen, J. Toppari, T. Suppula, J. Pekola, Fabrication of mesoscopic superconducting Nb wires using conventional electron-beam lithographic techniques, J. Vac. Sci. Technol., B: Microelectron. Nanometer Struct. 20 (1) (2002) 386–388, https://doi.org/10.1116/1.1445168.

[11] S. Samaddar, D. van Zanten, A. Fay, B. Sacépé, H. Courtois, C.B. Winkelmann, Niobium-based superconducting nano-device fabrication using all-metal suspended masks, Nanotechnology 24 (37) (2013) 375304, https://doi.org/10.1088/0957-4484/24/37/375304.

[12] T. Mcardle, K. Inderhees, P. Welander, A. Dove, J. Eckstein, Resistance in One-Dimensional Superconducting Epitaxial Niobium Nanowires, Ph.D. thesis University of Illinois at Urbana-Champaign, 2008.

[13] E.B. Gordon, A.V. Karabulin, V.I. Matyushenko, V.D. Sizov, I.I. Khodos, Production of ultrathin nanowires from refractory metals (Nb, Re, W, Mo) by laser ablation in superfluid helium, Laser Phys. Lett. 12 (9) (2015) 096002, https://doi.org/10.1088/1612-2011/12/9/096002.

[14] G. Cao, D. Liu, Template-based synthesis of nanorod, nanowire, and nanotube arrays, Adv. Colloid Interf. Sci. 136 (1-2) (2008) 45–64, https://doi.org/10.1016/j.cis.2007.07.003.

[15] A. Huczko, Template-based synthesis of nanomaterials, Appl. Phys. A Solids Surf. 70 (4) (2000) 365–376, https://doi.org/10.1007/s003390000440.

[16] C.R. Martin, Nanomaterials: a membrane-based synthetic approach, Science (New York, N.Y.) 266 (5193) (1994) 1961–1966, https://doi.org/10.1126/science.266.5193.1961.

[17] R.M. Penner, C.R. Martin, Controlling the morphology of electronically conductive polymers, J. Electrochem. Soc. 133 (10) (1986) 2206–2207, https://doi.org/10.1149/1.2108371.

[18] G.E. Possin, A method for forming very small diameter wires, Rev. Sci. Instrum. 41 (5) (1970) 772–774, https://doi.org/10.1063/1.1684640.

[19] C. Schönenberger, B.M.I. van der Zande, L.G.J. Fokkink, M. Henny, C. Schmid, M. Krüger, A. Bachtold, R. Huber, H. Birk, U. Staufer, Template synthesis of nanowires in porous polycarbonate membranes: electrochemistry and morphology, J. Phys. Chem. B 101 (28) (1997) 5497–5505, https://doi.org/10.1021/jp963938g.

[20] S. Senderoff, Electrodeposition of refractory metals, Int. Mater. Rev. 11 (January) (1966) 97–112, https://doi.org/10.1179/mtlr.1966.11.1.97.

[21] W. Simka, D. Puszczyk, G. Nawrat, Electrodeposition of metals from non-aqueous solutions, Electrochim. Acta 54 (23) (2009) 5307–5319, https://doi.org/10.1016/j.electacta.2009.04.028.

[22] V. Van, A. Silný, V. Daněk, Mechanism and kinetics of niobium ion reduction in LiFNaFK2NbF7 melts, Electrochem. Commun. 1 (8) (1999) 354–359, https://doi.org/10.1016/S1388-2481(99)00072-7.

[23] A.P. Abbott, K.J. McKenzie, Application of ionic liquids to the electrodeposition of metals, Phys. Chem. Chem. Phys. 8 (37) (2006) 4265–4279, https://doi.org/10.1039/B607329H.

[24] F. Endres, S. Zein El Abedin, Air and water stable ionic liquids in physical chemistry, Phys. Chem. Chem. Phys. 8 (18) (2006) 2101–2116, https://doi.org/10.1039/b600519p.

[25] P. Giridhar, S.Z. El Abedin, A. Bund, A. Ispas, F. Endres, Electrodeposition of niobium from 1-butyl-1-methylpyrrolidinium bis (trifluoromethylsulfonyl) amide ionic liquid, Electrochim. Acta 129 (2014) 312–317, https://doi.org/10.1016/j.electacta.2014.02.099.

[26] M. Mascia, A. Vacca, L. Mais, S. Palmas, E. Musu, F. Delogu, Electrochemical deposition of Cu and Nb from pyrrolidinium based ionic liquid, Thin Solid Films 571 (2014) 325–331, https://doi.org/10.1016/j.tsf.2014.05.030.

[27] S.Z. El Abedin, H. Farag, E. Moustafa, U. Welz-Biermann, F. Endres, Electroreduction of tantalum fluoride in a room temperature ionic liquid at variable temperatures, Phys. Chem. Chem. Phys. 7 (11) (2005) 2333–2339, https://doi.org/10.1039/B502789F.

[28] L. Mais, Electrodeposition of Nb, Ta, Zr and Cu From Ionic Liquid for Nanocomposites Preparation, Ph.D. thesis University of Cagliari, Italy, 2013.

[29] N. Elgrishi, K.J. Rountree, B.D. McCarthy, E.S. Rountree, T.T. Eisenhart, J.L. Dempsey, A practical beginner's guide to cyclic voltammetry, J. Chem. Educ. 95 (2) (2017) 197–206, https://doi.org/10.1021/acs.jchemed.7b00361.

[30] D.B. Williams, C.B. Carter, Transmission Electron Microscopy: A Textbook for Material Science, Springer, 1996.

[31] M. Murakami, T. Yogi, Strain in evaporated Nb thin films, J. Appl. Phys. 57 (2) (1985) 211–215, https://doi.org/10.1063/1.334790.

[32] W. DeSorbo, Effect of dissolved gases on some superconducting properties of niobium, Phys. Rev. 132 (1) (1963) 107, https://doi.org/10.1103/PhysRev.132.107.

[33] J. Halbritter, On the oxidation and on the superconductivity of niobium, Appl. Phys. A 43 (1) (1987) 1–28, https://doi.org/10.1007/BF00615201.

[34] K. Sokhey, S. Rai, G. Lodha, Oxidation studies of niobium thin films at room temperature by X-ray reflectivity, Appl. Surf. Sci. 257 (1) (2010) 222–226, https://doi.org/10.1016/j.apsusc.2010.06.069.

[35] D.M. Henry, S. Wolfley, T. Monson, B.G. Clark, E. Shaner, R. Jarecki, Stress dependent oxidation of sputtered niobium and effects on superconductivity, J. Appl. Phys. 115 (8) (2014) 083903, https://doi.org/10.1063/1.4866554.

[36] J. Bellina Jr, R. Lederich, J. O'Neal, Variation of concentration with depth of absorbed oxygen in niobium during oxidation, J. Appl. Phys. 43 (2) (1972) 287–292, https://doi.org/10.1063/1.1661109.

[37] H. Shiraishi, K. Furuya, R. Watanabe, Change in solute oxygen level and loss of ductility of niobium during oxidation in imperfect vacuum conditions, J. Less Common Met. 63 (2) (1979) 147–158, https://doi.org/10.1016/0022-5088(79)90239-X.